Modeling of Radial and Tangential Roebel Bar Force Distributions in Large Electrical Machines Considering Longitudinal Transposition

Amir Ebrahimi and Marius Meiswinkel

1 Introduction

Studying large electrical machines is an ongoing important topic due to the very different electromagnetic phenomena and modeling uncertainties caused by their immense dimensions. Despite decades of developing calculation methods for megawatt generators, there are still varieties of problems and aspects to be studied [1]. The necessity of extending our understanding of operational characteristics of large generators can be described considering design and operational challenges of these systems. Regarding design aspects, a more comprehensive model results into a better design with more optimization possibility. Regarding reliability, a comprehensive model describes the multi-physical relations between several parameters more sophisticatedly and results in more deterministic lifetime models and improves the maintenance management and reduces outages and costs. Roebel bar forces are a suitable example to explain this fact. The slot stray fluxes generate double frequency radial and tangential forces on the Roebel bars in large generators. These vibrations could lead to bar deformation, deterioration of isolation and fixation materials in the slot, and in the worst case, it results in sub-conductor or conductor short circuits to the stator core or to each other. A comprehensive model of Roebel bar forces helps to understand the behavior of these forces for a better design of slot materials and a sophisticated anticipation of Roebel bar condition.

Since these forces are much less than the radial double frequency forces acting on the stator core and teeth, they are not comprehensively considered in the literature. In general, a simplified formulation based on the Lorentz force formulation is given for the slot ground force estimation. The tangential force on the slot wall is usually neglected. Grabner et al. gives an analytical approximation of displacement

A. Ebrahimi (✉) · M. Meiswinkel
Leibniz University, Hannover, Germany
e-mail: ebrahimi@ial.uni-hannover.de

of Roebel bar and mechanical stress in the slot of large generators [2, 3]. Pantelyat et al. investigates the forces on the slot wedges [4].

In this chapter, an investigation on the tangential and radial Roebel bar forces considering bar transposition is proposed. In the first section, the origination and formulation of Roebel bar forces are given. After that the tangential and radial stray fluxes in the slot are described, and the impact of the field and stator current on these fluxes are explained. This section is followed with an investigation on the impact of the load angle and power factor on the slot fluxes. At the end, the radial and tangential forces are estimated both for a single transposed sub-conductor and for a Robel bar. Finally, these values are calculated and discussed for a real hydrogenerator.

2   Roebel Bar Forces

The origin of Roebel bar forces is widely independent from the generator type. Nevertheless, to concretize the investigation and generate specified and comparable results, the origination of Roebel bar forces in a salient pole hydrogenerator is studied in this chapter.

2.1   *Salient Pole Synchronous Generator with Roebel Bar*

Schematic of one pole pitch of a salient pole generator is indicated in Fig. 1. The main parts of the generator are: rotor pole with damper winding, rotor rim, tee head attachment, pole winding, stator yoke and teeth, and the stator windings (Roebel bars). The DC current in the rotor winding generates a magnetic flux which closes its path mainly through rotor body, air gap, teeth, and yoke. The shaft of the generator is connected to a prime mover (in this case a hydroturbine). The shaft rotation creates a rotating magnetic field in the air gap and induces a three-phase voltage in
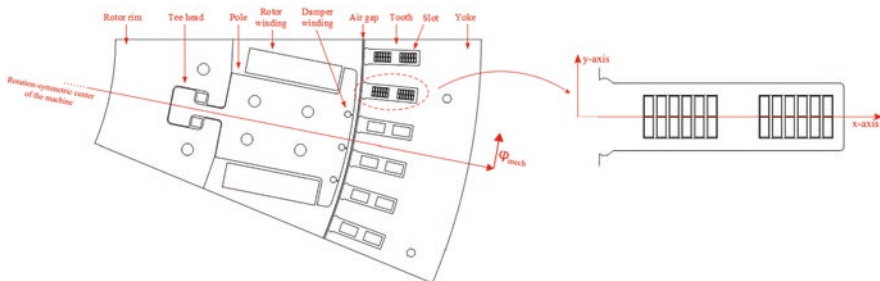

Fig. 1 Schematic of a salient pole generator; (**a**) left: one pole pitch, (**b**) right: one slot with sub-conductors

the stator windings. The parameters of the generator simulated in this chapter are summarized in Table 1.

The rotor winding generates an almost sinusoidal field across the air gap. Considering the spatial distribution of the air gap flux density, one can observe breakdowns in the flux density under the slots. The average air gap flux density can be estimated with carter factor. A small portion of the air gap flux lines enters into the slot radially and takes a circular path and enters the tooth tangentially. The conductor in the slot also generates fluxes across the slot with a dense concentration at the slot opening. These two flux densities are responsible for the radial and tangential forces on each sub-conductor in a Roebel bar.

Alternating current creates an alternating flux in the conductor material and causes a skin effect. To reduce the eddy current losses in the conductors, the conductors are divided into sub-conductors, which are connected together just at the beginning and at the end of the winding. To eliminate the circulating currents in the sub-conductors, every parallel-connected sub-conductor has to be surrounded exactly by the same amount of slot stray flux [5]. This is done by transposing the sub-conductors and use of Roebel bars. A schematic of the Roebel bar is illustrated in Fig. 2.

2.2 Lorentz Force and Maxwell Stress Tensor

The tangential (y-direction) and radial (x-direction) stray fluxes densities in the slot generate a radial and a tangential force on the current-conducting Roebel bar acting on the slot ground and slot wall, respectively. The reformulation of Lorentz force describes these forces. Assuming $q = \rho V$ and substituting with $\vec{J} = \rho \vec{v}$ in the Lorentz force definition $\vec{F} = q\vec{v} \times \vec{B}$, the force can be given by:

$$\vec{F} = \iiint \vec{J} \times \vec{B} dV$$

(1)

The variables in Eq. 1 can be determined using Finite Element Methods (FEM) in the slot of a generator. However, the current density $\vec{J}$ and the flux density $\vec{B}$ are

Table 1 Machine parameter

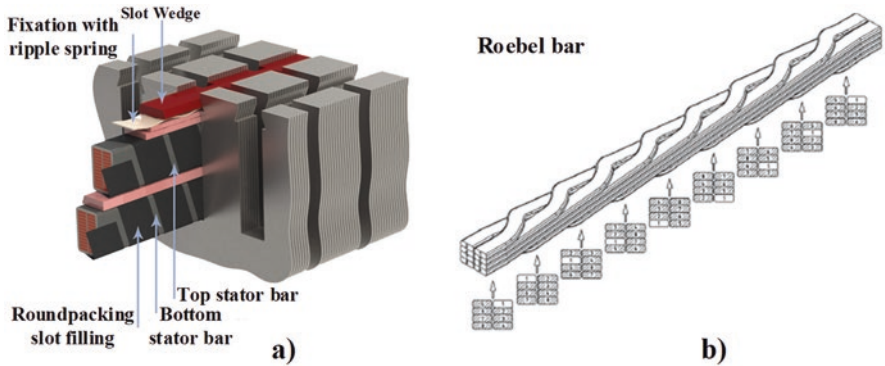| Parameter	Value
Rated voltage	550 V Y
Rated current	768 A
Rated torque	18.6 KNm
Rated speed	375 rpm
Number of poles	16
Number of slots	96
Max. Power	880 kW

Fig. 2 Cross section of the stator with conductors in a slot; (**a**) two layer conductors and (**b**) transposed Roebel bar. (Source of images: (**a**) https://www.fortum.se (**b**) M. Znidarich, "Hydro Generator High Voltage Stator Windings")

not constant along the z-direction in the generator because of the cooling ducts. Therefore, it is necessary to divide the conductor along the z-direction into smaller segments (1 mm). The force on the segment $d\vec{s}$ of the conductor is given by:

$$\vec{F} = A\vec{J} \times \vec{B}(s) d\vec{s} \tag{2}$$

where A is the cross section of the sub-conductor. Since the length of the sub-conductors is much more than its cross section, Eq. 2 can be simplified by:

$$\vec{F} = \sum lA\vec{J} \times \vec{B} \tag{3}$$

To consider the transposition of the sub-conductors in the z-direction, all three components of the current density should be estimated. This can be given by [6]:

$$\vec{J} = \begin{pmatrix} J_x \\ J_y \\ J_z \end{pmatrix} = \begin{pmatrix} cos\beta & 0 & sin\beta \\ sin\alpha\ sin\beta & cos\alpha & -sin\alpha\ cos\beta \\ -cos\alpha\ sin\beta & sin\alpha & cos\alpha\ cos\beta \end{pmatrix} \begin{pmatrix} 0 \\ 0 \\ J_z \end{pmatrix} \tag{4}$$

where α and β are the unit area vectors in y and x direction given by:

$$\alpha = \arcsin\left(\frac{dy}{dz}\right), \beta = \arcsin\left(\frac{dx}{dz}\right) \tag{5}$$

FEM programs mostly estimate the magnetic forces based on Maxwell Stress Tensor (MST). Therefore, it is necessary to compare these two force calculation methods. The MST can also be derived from Lorentz force using Maxwell

equations and Vector Potential formulation [7]. The modified (MST) method used in FEM programs (e.g., FEMM) applies multiple integrating lines in a path including the sub-conductors. This path is selected merely in materials with the unit permeability due to the derivation of MST. The MST formulation to calculate the forces on the conductors in FEMM is given by [8]:

$$F_j^{\Omega a} = \frac{1}{\mu_0} \int_{\Gamma - \delta\Omega_b} (g_- - g_+) \left[(B.n) B - \frac{1}{2} B^2 n \right] ds + \sum_{k=1}^{q} \frac{1}{\mu_0} \int_{\Omega_{bk}} \left[\frac{1}{2} B^2 \Delta g - (B.\Delta g) B \right] dV \quad (6)$$

where Ω_{bk} are the inner integrating loops in Ωa and g is a piecewise differentiable function [9]. The difference between Lorentz force and MST for calculating conductor forces in a slot is just 0.01%. Hence, all forces in this chapter are estimated with Lorentz force formulation.

3   Radial and Tangential Flux Density Distribution in the Slot

Since conductor forces occur with respect to the radial and tangential components of flux density in the slot B_x and B_y, the distribution of these flux densities is described in this chapter. Considering Fig. 3a–c, it can be observed that B_x is higher in the slot opening region, since B_x is mainly caused by the rotor current. The influence of the rotor field on the B_x is less than the winding current at the upper conductor. The clockwise rotating magnetic field originated from the current of the upper conductor (shown with red circle in Fig. 3a), causing an increase in B_x at the upper side of the conductor which can also be observed in Fig. 3c. After half electric period, this magnetic field will be higher at the lower side of the conductors. As it can be observed from Fig. 3d–f, the influence of the rotor field in B_y is negligible. The tangential flux in a slot is mainly due to the phase currents. It generates a force F_y on the slot wall. B_y is bigger at the slot opening. The kink in the Fig. 3e shows the influence of the radial field around the conductor on the tangential field in the slot. Each sub-conductor causes a kink in the flux density distribution. Furthermore, the flux lines leave the lower side of the slot perpendicularly but enter the tooth on the upper part of the slot with an angle.

Flux density distribution should also be analyzed for a mix slot in which the upper and lower bars belong to two different phases. It can be shown that the behavior of the radial and tangential flux densities in a slot remains similar to a normal slot in which both the upper and the lower conductors belong to the same phase. It can also be observed that B_x is the same for a normal and a mix slot, since B_x originates mainly from the rotor field. The behavior of B_y remains also similar to a normal slot; however, the amplitudes are less for a mix slot.
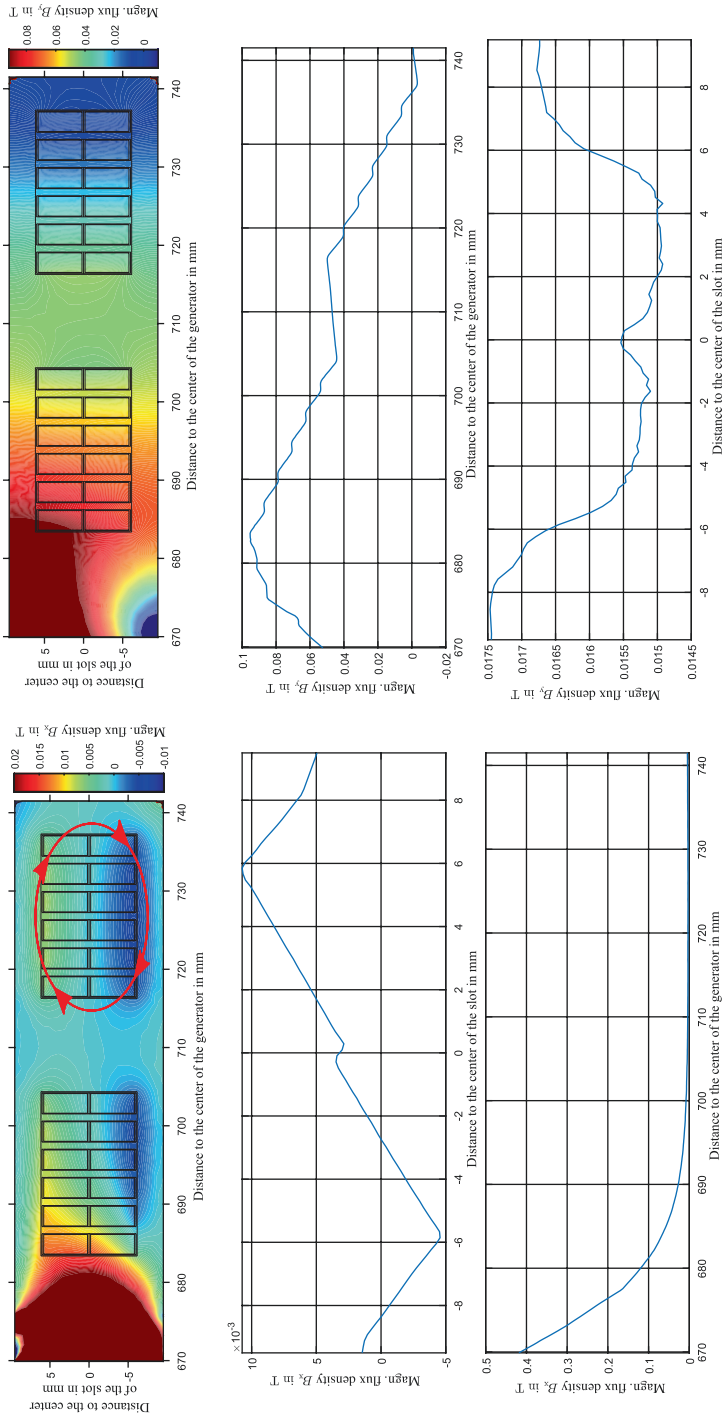
Fig. 3 Flux density distribution in the slot: (**a**) B_x distribution in a slot, (**b**) B_x as a function of slot width at the distance of 729 mm to the center of the machine, (**c**) B_x as a function of slot height, (**d**) B_y distribution in a slot, (**e**) B_y as a function of slot width at the distance of 729 mm to the center of the machine, (**f**) B_y as a function of slot height

3.1 Impact of Field Current on the Flux Density Distribution in the Slot

Field current is mainly responsible for generating B_x. This can be observed in Fig. 4. B_x is calculated for different rotor positions and currents. The kinks in the diagrams in Fig. 4a are due to the asymmetrical damper winding on the surface of the pole. Also the influence of rotor core saturation can be observed in Fig. 4. More interesting is the behavior of B_y. The increase in the flux density can be explained by the stator core saturation. In this case, the teeth are saturated and the difference between the slot and tooth reluctance is less. Therefore, more flux lines enter into the slot, rotate, and enter the tooth through the slot wall. To describe the behavior of the flux density in Fig. 4c, we need to consider the relative position of the rotor to the middle of the slot. As the rotor rotates counterclockwise (Fig. 1), B_y increases at first, and then decreases as the middle of the pole is aligned with the middle of the slot (same B_y to the left and right side of the slot). After that, the rotor starts leaving the slot area and the second maxima happens since the south pole enters the slot area. This double frequency phenomenon develops the main part of the forces on the Roebel bar in the slot.

3.2 Impact of the Stator Current on the Flux Density Distribution in the Slot

The influence of the phase current on B_y is linear, since B_y mainly depends on the phase current. However, B_x in a slot with let say phase "w" is 90° leads to the phase current. To explain this, we need to consider the two other phases. When the current in phase "w" is maximum, the field lines of this phase goes through the phases "-u" and "v". This field develops a considerable B_y in the slot with phase "w". When the current in phase "w" is zero, the currents in phase "u" and "w" generate a magnetic. Consequently, this field contributes considerably to B_x in the slot with phase "w" which is the field passing through the same slot reason for 90° leading behavior of B_x and the phase current angle.

4 Impact of Operation Points on the Roebel Bar Forces

4.1 Impact of Load Angle on the Flux Density Distribution in the Slot

The load angle δ is defined as the angle between phase voltage V and the induced voltage E and is an important parameter for determining the torque of a salient pole machine given by:
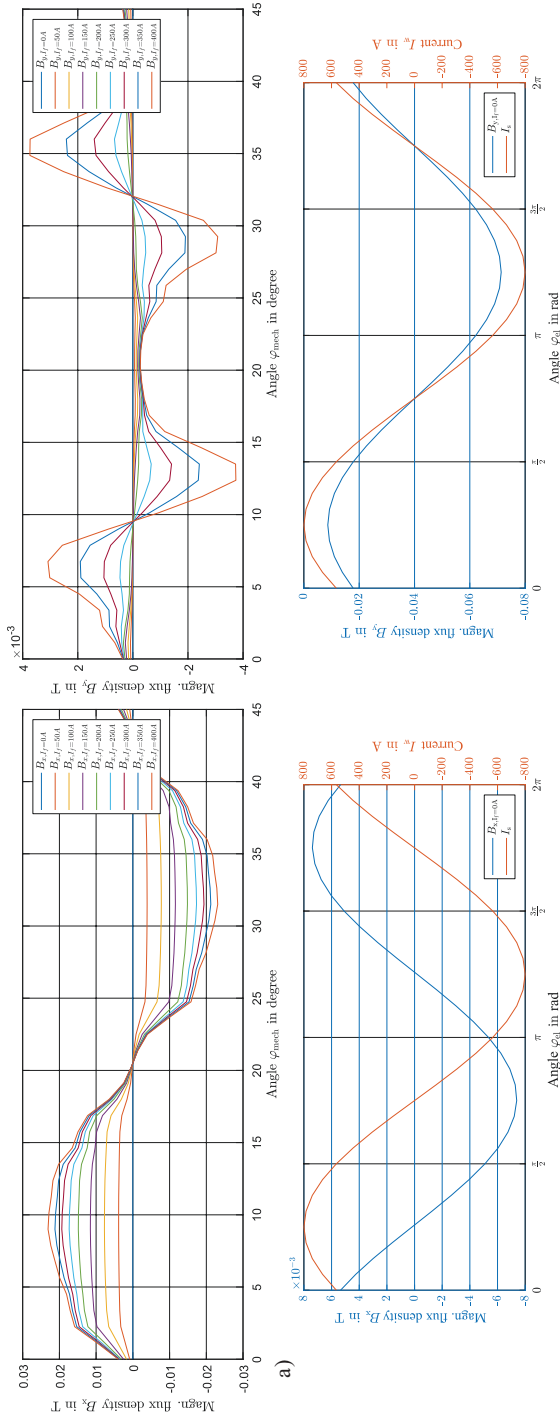
Fig. 4 Impact of the field current on the flux density distribution in the slot

$$T = \frac{m}{2\pi n_0} \left(\frac{VE}{X_d} \sin(-\delta) + \frac{V^2}{2} \left(\frac{1}{X_q} - \frac{1}{X_d} \right) \sin(-2\delta) \right) \tag{7}$$

where X_d and X_q are the inductances in the d- and q-axis. Since B_y mainly depends on the phase current, it is expected that the load angle has no major impact on the forces acting in the direction of the slot ground F_x as it can be observed in Fig. 5b. F_x is a double frequency force acting on the slot ground with a constant polarity.

On the other hand, the radial flux density in the slot B_x depends mainly on the load angle as it can be observed from Fig. 5c ($\varphi_{el} = p\varphi_{mech} + \delta$). The change in the amplitude is caused by the salient pole. The total MMF current can be calculated by transforming the rotor current I_f to the stator side I'_f and adding them to the stator current ($I_m = I_s + I'_f$). Now the total MMF can be given by:

$$V_m = \frac{\sqrt{2}}{\pi} \frac{m_s}{p} N_s k_w I_m \cos\left(\frac{x_r}{\tau_p} \pi \right) \tag{8}$$

where N_s and k_w are the stator winding number and factor. τ_p is the pole pitch and x_r is the distance to the middle of the pole. Thus, it is possible to give an approximation of the air gap flux density with:

$$B_h(x_r) = \mu_0 \frac{V_m(x_r)}{\delta(x_r)} \tag{9}$$

where $\delta(x_r)$ describes the air gap reluctance. Equation 9 describes the air gap flux density referring to the rotor position which can be referred to the stator with:

$$x_r = \frac{2\pi r_r}{360°} (\varphi_{mech}) \tag{10}$$

Based on Eq. 9, estimated flux densities for different load angles create an idealized form of the fields indicated in Fig. 5c. One way to generate the exact B_x diagrams of Fig. 5c is to apply conformal mapping to Eq. 9.

4.2 Impact of Power Factor on the Flux Density Distribution in the Slot

Power factor relates to the angle between stator current and voltage, and it could be also shown that it is connected to the load angle with:
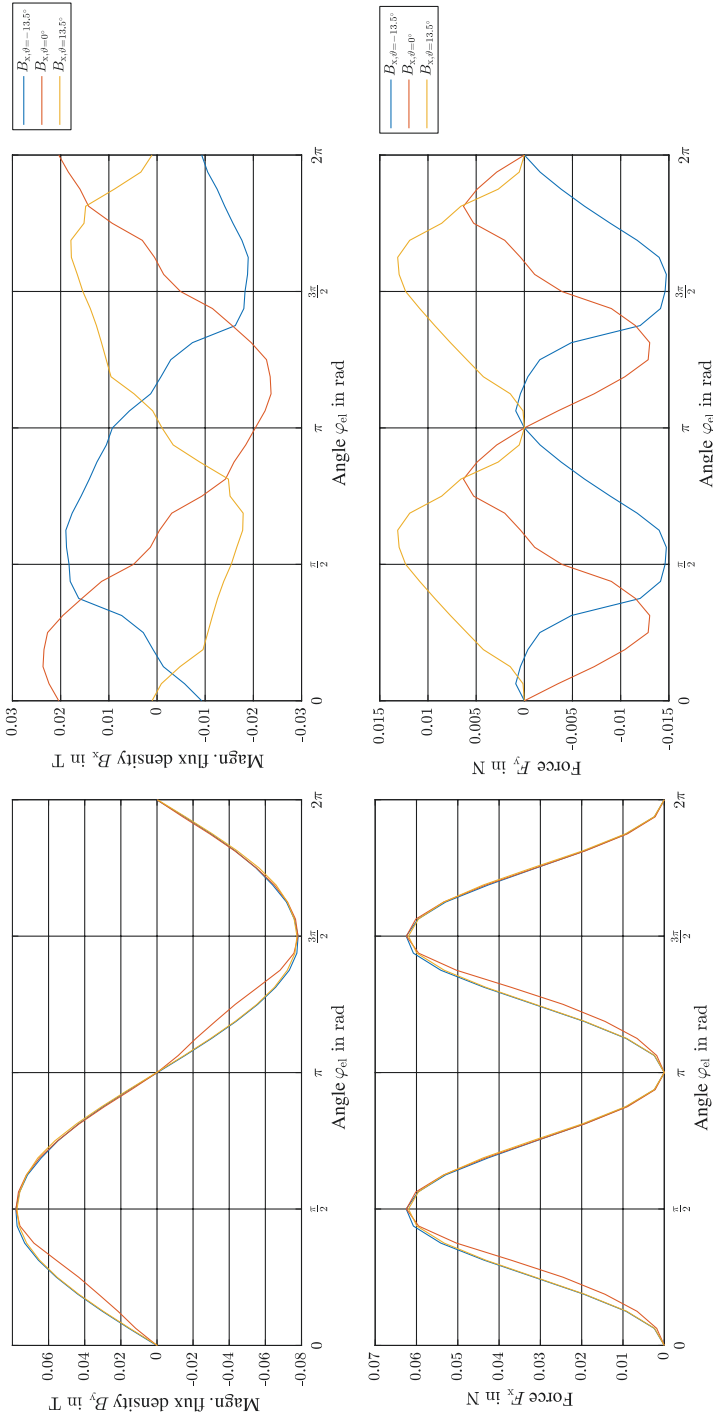
Fig. 5 Impact of load angle on Roebel bar forces: (**a**) B_y vs. δ, (**b**) F_x vs. δ, (**c**) B_x vs. δ, (**d**) F_y vs. δ

$$\tan\left(\delta\right) = \frac{r_s I_m \sin\left(\varphi\right) + \omega_e L_q I_m \cos\left(\varphi\right)}{V_m + r_s I_m \cos\left(\varphi\right) - \omega_e L_q I_m \sin\left(\varphi\right)} \tag{11}$$

According to Fig. 6b, power factor shifts F_x but does not change its amplitude. Since B_y is mainly caused by the phase currents, its magnitude remains constant and just a phase shift in the radial force can be observed. However, the tangential forces are more subject to variation since the B_x component of the flux density in the slot depends on the rotor position. Considering the relation between the load and power angle described by Eq. 11, the power factor influences the tangential Roebel bar forces more drastically. While the force is positive for $\cos(\varphi) = 0$, it is shifted down for other values as it can be observed in Fig. 6a.
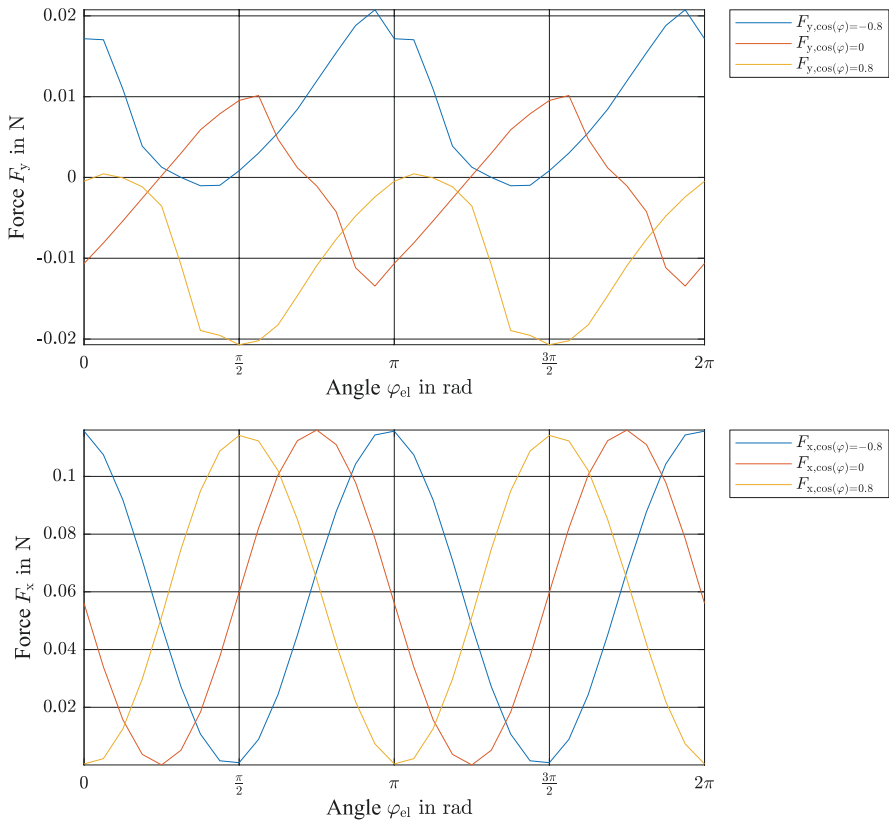

Fig. 6 Radial and tangential Roebel bar forces as a function of power factor

5 Radial and Tangential Forces on the Roebel Bar

5.1 Sub-conductor Forces

As mentioned in Sect. 3, the flux density in a slot is not constant across the slot and varies across different positions in the slot. Therefore, the radial and tangential forces on the sub-conductors are also functions of their position in the slot. Generally, it can be said that the sub-conductors closest to the slot opening experience much more radial and tangential forces than the sub-conductors near to the slot ground. The force distribution is similar to Fig. 3. To estimate the total force on a sub-conductor, a transient 3D-FEM model of a generator with sub-conductors is constructed (Fig. 7).

The simulation results for a rotor field current of 260 A and the stator current of 800 A are indicated in Fig. 8.

The results are similar to 2D simulation. However, the 3D-FEM estimated forces are less than the multiplication of 2D-FEM results with the length of the machine.
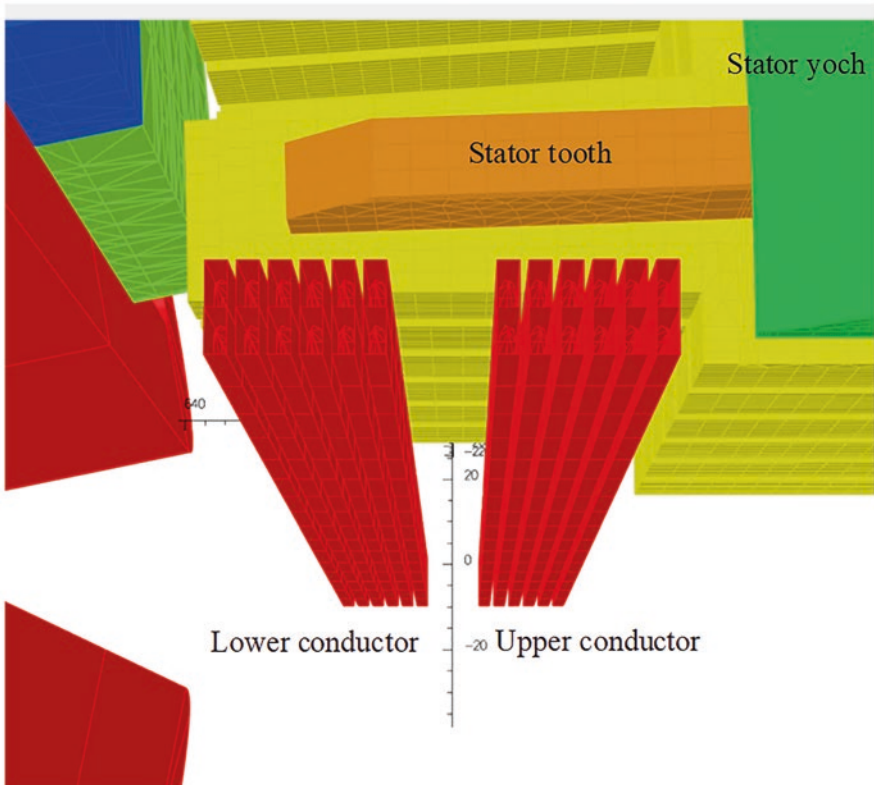

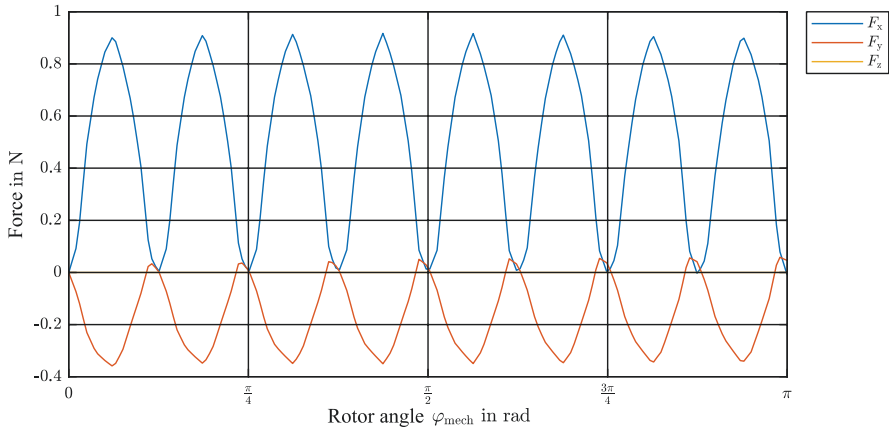**Fig. 7** 3D-FEM Model for calculating the sub-conductor forces

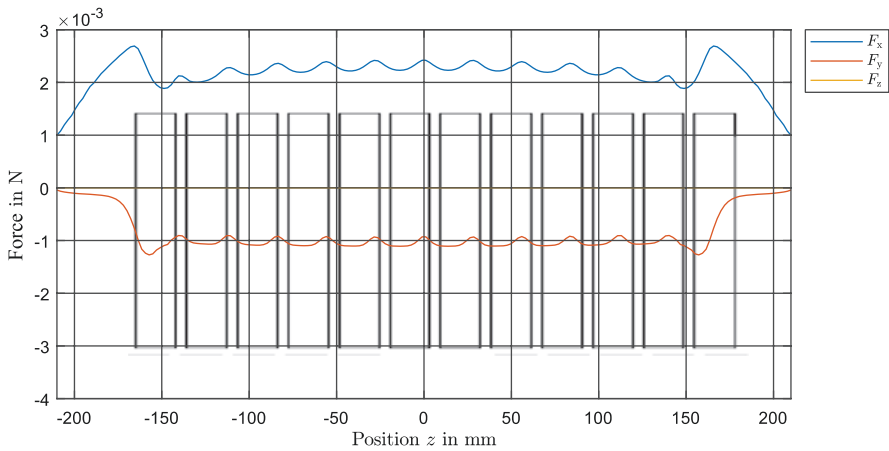**Fig. 8** Total sub-conductor forces as a function of mechanical angle

Fig. 9 Sub-conductor forces as a function of the positions along the z-axis

To explain this, one should consider each segment of a sub-conductor along the z-axis. The 3D behavior of sub-conductor forces are determined by several factors. The breakdowns in the F_y component relate to the cooling ducts in the stator. The magnetic reluctance in the cooling ducts is much bigger than that in the stator core. Hence, the air gap flux density under cooling ducts is less than in the active part of the machine which can be estimated with Carter factor. Therefore, the B_x component of the flux density is less and consecutively the F_y component breaks down in this region. More interesting is the impact of the cooling ducts on the slot ground forces. Under the cooling ducts, the flux lines take a circular path and enter into the stator core along the z-direction, perpendicularly to the radial fluxes in the tooth. This circulation of flux lines increases B_y and, consecutively, F_x is even more than the active region, which can be observed in Fig. 9.

The same effect can also be observed at the end region. Due to an increase in radial and tangential components of the flux density in this region relating to the fringing effect, an increment in the tangential and radial forces can be recognized (Fig. 9). Although the force development in a slot has the same behavior in 2D and 3D, for correct estimation of sub-conductor forces a 3D calculation is essential.

5.2 The Impact of Transposition

As it can be recognized in Fig. 3, the flux density distribution in the slot is not homogenous and hence the position of the sub-conductor in a slot has an impact on the forces acting on this sub-conductor. The current density in each segment (1 mm) is estimated with the method described in Sect. 2.2. The integral volume is the volume of the sub-conductor segment. B_x and B_y components of flux density in the slot along the z-axis are calculated with the 3D-FEM. While the sub-conductors closest to the rotor experience much more forces, the forces near the slot ground are much less. The rotor has almost no influence in the slot ground region; however, the radial component of the conductor field acts on the sub-conductors. While the lower conductor is pushed through the upper slot wall, the upper conductor is pushed through the lower slot wall. Figure 10 shows the forces acting on single sub-conductor as a function of positions along the z-axis. A difference between a Roebel bar and a straight bar can be recognized comparing to Fig. 9. Considering F_x, there is a sudden increment in the force, because in this moment the sub-conductor changes its position. The position of a sub-conductor changes along the z-axis. The radial forces decrease as the sub-conductor moves through the slot ground. Due to this change of position, a small F_z component can be recognized in Fig. 10. The same is also valid for F_y; however, a change in the force polarity can be observed in the middle of the machine since the sub-conductor transposition moves through the other half of the bar.
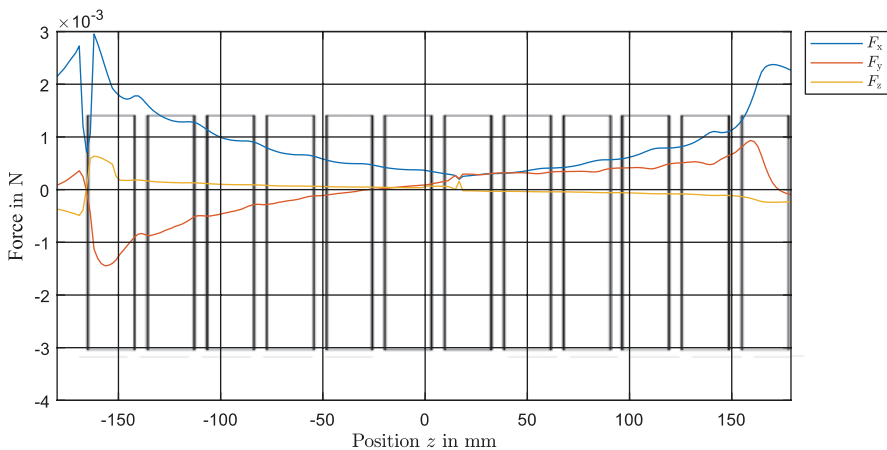

Fig. 10 Forces acting on single sub-conductor as function of positions along the z-axis

For a real generator with a diameter of 18 m, 2253 A current in the stator bar and 1.2 T air gap flux density, the forces against the slot wall would be 23 N for the lower conductor and 5 N for the upper conductor. Approximately $F_x = 60$ N acts on the upper conductor with double frequency. This should be considered by design of isolation and fixation materials in the slot.

6   Conclusion

A comprehensive study of Roebel bar forces in large generators is proposed in this chapter. The impact of the radial and tangential flux lines in the slot and the radial cooling ducts on the three-force Roebel components are investigated. Moreover, the impacts of load angle and power factor on these forces are studied. The estimations are performed with a 3D-FEM model, and the effect of Roebel bar transposition is considered. The behavior of the forces along the machine length is investigated. The radial and tangential Roebel bar forces for a real hydrogenerator are estimated. Since the relation and amplitude of radial and tangential forces change in different operation points, a mechanical analysis should be performed to estimate the mechanical deterioration of Roebel bar, fixing and isolation materials due to the radial and tangential Roebel bar forces.

References

1. A. Ebrahimi, *Characterization of a Large Electrical Machine Test Bench for Advanced Investigations on Wind and Hydro Generators*, 4th IEEE Southern Power Electronics Conference, Dermatol. Sin., pp. 1–6, December 2018
2. C. Grabner, E. Schmidt, *Analytical Approximation of the Displacement Process of Roebel Bars*, Conference Record – IAS Annual Meeting (IEEE Industry Applications Society), February 2002
3. C. Grabner, H. Köfler, *Mechanical Stress Behavior Inside Slots of Large Hydro Generators*. https://doi.org/10.24084/repqj01.313
4. M.G. Pantelyat, O. Biri, A. Stermecki, *Electromagnetic Forces in Synchronous Turbogenerator Rotor Slot Wedges*, Proceedings of the Joint INDS'11 & ISTET'11, Austria, July 2011
5. J. Pyrhönen, et al., *Design of Rotating Electrical Machines*. Wiley. ISBN: 978-0-470-69516-6
6. O. Marti, M. Gonçalves, *Lecture notes PHYS2200.0*, Darmstadt, Ulm University, Institute for Experimental Physics, 2018, http://wwwex.physik.uni-ulm.de/lehre/ap-2015/ap-2015.pdf
7. A. Ebrahimi, *Hybrid Analytical Modeling and Optimization of Surface Mounted Permanent Magnetic Synchronous Motors Considering Spatial Harmonics*, Dissertation, ISBN: 978-3-8440-5026-4
8. D. Meeker, *Finite Element Method Magnetics*. Version 4.2, 2018, http://www.femm.info/wiki/Files/files.xml?action=download&file=manual.pdf
9. S. McFee, J.P. Webb, D.A. Lowther, A tunable volume integration formulation for force calculation in finite-element based computational magnetostatics. IEEE Trans. Magn. **21**, 439–442 (1988)